



Cite this: *Soft Matter*, 2024, 20, 8997

# Liquid crystalline collagen assemblies as substrates for directed alignment of human Schwann cells†

Homa Ghaiedi,<sup>a</sup> Luis Carlos Pinzon Herrera,<sup>b</sup> Saja Alshafeay,<sup>c</sup> Leonard Harris,<sup>c</sup> Jorge Almodovar <sup>b</sup> and Karthik Nayani <sup>\*,a</sup>

Collagen is a key component of the extracellular matrix (ECM) and well-oriented domains of collagen are important for mimicking the local cell environment *in vitro*. While there has been significant attention directed towards the alignment of collagen, formation of large-scale oriented domains remains a key challenge. Type I collagen self-assembles to form liquid crystalline (LC) mesophases in acidic conditions at concentrations above 100 mg mL<sup>-1</sup>. The LC mesophase provides an efficient platform for large-scale alignment and patterning of collagen coated substrates. However, there still exist challenges related to solubilizing and processing of collagen at such high concentrations in order to replicate the native ECM. In this contribution, we report on centimeter-scale alignment in collagen-coated glass substrates using solutions that are well below the LC-forming concentrations. Importantly, we are also able to extend this method to macroscopic 3-D LC-collagen hydrogels with programmed anisotropy within them to create a mimic of the native ECM. We show that the orientation and aspect ratio of human Schwann cells are strongly coupled with the alignment of the collagen substrate/hydrogel. We use a simple model to estimate the critical magnetic field strength needed for a given concentration of collagen to permit macroscopic alignment-enabling guidance for future studies on alignment of collagen at high concentrations.

Received 3rd May 2024,  
Accepted 25th October 2024

DOI: 10.1039/d4sm00534a

[rsc.li/soft-matter-journal](https://rsc.li/soft-matter-journal)

## 1. Introduction

Regeneration of damaged peripheral nerve, due to trauma or neurological disease, impacts approximately 20 million people in the US and corresponds to an annual healthcare expense of approximately \$150 billion.<sup>1,2</sup> Nerve guide conduits (NGCs) are becoming more prominent as a substitution for autologous allografts as they eliminate the need for multiple surgeries to harvest the autologous tissue.<sup>3,4</sup> NGCs have shown great promise in the regeneration of short nerve defects; however, they fail in the regeneration of large nerve defects due to the lack of guidance cues which can deterministically proliferate nerve cells.<sup>3,4</sup> An approach to address this challenge is by using templated substrates as NGCs that are capable of imparting

guidance cues for the growth and proliferation of human Schwann cells (HSCs).<sup>3,5</sup> We wager that LCs (fluids with orientational order) provide an efficient platform to design NGCs incorporating well-defined orientational cues.<sup>3,6–8</sup> Our hypothesis is inspired by findings that collagen self-assembles within the body to form a myriad of LC phases.<sup>9,10</sup> From a fundamental perspective, our study also aims to probe the coupling of substrate anisotropy and reconfiguration of cells in response to mechanical cues. Our work advances biologically inspired design of LC-based substrates and hydrogels with internal ordering and properties that can be finely tuned, enabling directional growth of cells.

HSCs play a vital role in the regeneration of peripheral nerve through secretion of various proteins that affect the behavior of glial cells in formation of cellular channels that are responsible for guiding axons to the correct targets.<sup>11</sup> The orientational fidelity of HSCs promotes axonal outgrowth, which in turn controls their orientation.<sup>12,13</sup> Therefore, understanding the fundamental principles by which the directional behavior of HSCs can be mediated is necessary. Several reports have focused on the effects of spatial configuration of the extracellular matrix (ECM) on the alignment of various biological cells including HSCs.<sup>3,14–17</sup> There are only a few studies

<sup>a</sup> Ralph E. Martin Department of Chemical Engineering, University of Arkansas, 3202 Bell Engineering Center, Fayetteville, AR, 72701, USA.  
E-mail: [knayani@uark.edu](mailto:knayani@uark.edu)

<sup>b</sup> Department of Chemical, Biochemical, and Environmental Engineering, University of Maryland Baltimore County, Baltimore, MD, 21250, USA

<sup>c</sup> Department of Biomedical Engineering, University of Arkansas, Fayetteville, AR, 72701, USA

† Electronic supplementary information (ESI) available. See DOI: <https://doi.org/10.1039/d4sm00534a>



associated with the role of alignment/orientation of the substrate and their influence on HSCs.<sup>5</sup> Moreover, these studies are primarily limited to 2D environments that are incapable of mimicking the native ECM. 2D environments are insufficient to replicate the native environment as, the growth pattern of cells is highly influenced by the topography of ECM.<sup>18–20</sup> Changes in the morphology of cells upon exposure to constraints of a 2D environment affect the proliferation rate, signaling and secretion.<sup>21</sup> Alteration of phenotypic properties and loss of polarity due to the poor interaction with ECM in 2D environments can also to an insufficient response to apoptosis.<sup>22</sup> The intracellular interaction in the native environment also has enormous impact on the epithelial collagen production and regulation of intercellular events.<sup>23</sup> Therefore, it is important to have a 3D environment that can imitate the native ECM if any extracellular event is to be accurately investigated.

The spatial arrangement of ECM plays a vital role in controlling the behavior of biological cells.<sup>24–26</sup> Collagen as a major component of native ECM has shown to self-assemble into chiral nematic LC structures at concentrations above  $100 \text{ mg mL}^{-1}$ , enabling cells to anchor to and elongate along the long axis of the composed fibrils.<sup>9,10,27–31</sup> Additionally, the alignment of LCs can be triggered by several stimuli including flow, electric or magnetic field, and underlying alignment layers.<sup>32–35</sup> In this study, we aim to investigate how a mimic of native-ECM using well-aligned collagen networks can affect the directional orientation and spread of HSCs. To achieve this, it is critical to develop facile methods to prepare films and hydrogels constituted of anisotropically arranged collagen and subsequently, to investigate the orientational behavior of HSCs cultured in such environments.

Here, we harness the inherent anisotropic viscoelastic properties and diamagnetic susceptibility of collagen to create novel platforms composed of long-range unidirectionally aligned cholesteric bands (at concentrations well below the reported critical concentration of collagen to create LC phase), both in films and hydrogels and study the effect of anisotropy on the alignment and spreading of HSCs. While the alignment of HSCs along the direction of collagen orientation is intuitively expected, our results also show that, remarkably, the aspect ratio of HSC is a function of the alignment of collagen.

## 2. Results and discussion

Understanding the process driving the formation of liquid crystalline collagen enables greater control over the configuration of these assemblies, ultimately enabling the design of scaffolds that are more fitting for specific applications.<sup>6–10,16,36–38</sup> Collagen type I is composed of three polypeptide chains wound together in a left-handed triple helix (depicted in Fig. 1A). Collagen self-assembles into fibrils with diameter of 1 nm and length of 300 nm. At low concentrations, collagen exists in an isotropic phase characterized by the absence of a preferred orientation of the constituent collagen fibrils. Upon increasing the concentration above  $100 \text{ mg mL}^{-1}$  in acidic environments ( $\text{pH} = 2.5–3$ ),

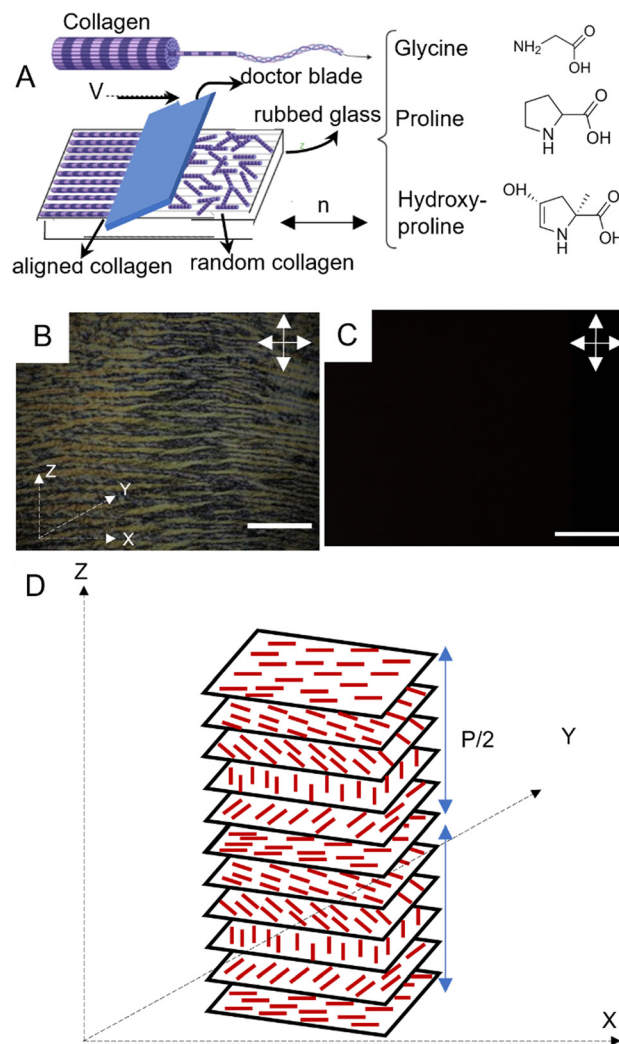


**Fig. 1** (A) Schematic demonstration of shear-driven alignment of collagen on rubbed PI coated substrate. Collagen solution was deposited using a doctor blade upon which a film composed of unidirectionally aligned cholesteric bands formed spontaneously. (B) Cross-polarized optical micrograph of LC collagen ( $10 \text{ mg mL}^{-1}$  in aqueous acetic acid ( $\text{pH} 2.5$ ) film, which has been coated on a PI-coated glass substrate that was previously rubbed to induce directional alignment. The characteristic pattern of alternating light and dark bands, known as cross-striations, is clearly visible in the cholesteric bands. (C) Cross-polarized optical micrograph of collagen solution (with the same concentration and  $\text{pH} 2.5$ ) between a coverslip and a microscope glass spaced by  $150 \mu\text{m}$ , serving as a control to evaluate the effect of shear on the alignment of cholesteric bands. (The scale bar represents  $100 \mu\text{m}$  in both (B) and (C)). (D) Schematic of arrangement of collagen molecules exhibiting a left-handed twist across parallel planes. The distance between layers, denoted as  $P$  is equal to the full rotation of the long axes at  $360^\circ$ , and it is known as the pitch. The double-sided arrows indicate the direction of analyzer and polarizer.

however, collagen demonstrates liquid crystalline behaviour, as evidenced by the formation of oriented cholesteric bands composed of fibrils arranged in a hexagonal packing pattern.<sup>10,39</sup> The directional preference seen in liquid crystals arises from the collective behaviour of macromolecular assemblies comprised of asymmetrical molecules. This is consistent with an Onsager-like description wherein the LC-phase arises



from interplay between orientational entropy and excluded volume.<sup>40</sup> The system seeks to balance the need to maximize the overall entropy by increasing its positional entropy and sacrificing its orientational freedom, leading to the formation of the LC phase.

### 2.1. Preparation and characterization of aligned collagen films with microgrooves and shear

Polyimide (PI) coated glass surfaces that are rubbed uniaxially to create microgrooves are a well-established method to create well-defined alignment in LC films.<sup>41,42</sup> In this vein, we create aligned collagen films using a combination of PI-coated glass substrates and shear force. The motivation to use shear-driven alignment stems from the objective to use concentrations of collagen that are well-below LC forming concentrations.<sup>43</sup> Shear-driven alignment was achieved using a doctor blade to deposit collagen solutions (with concentrations as low as 10 mg mL<sup>-1</sup>) on glass substrates. Prior to the deposition process, microgrooves were formed on PI-coated microscope glasses, by rubbing the glass in a unidirectional manner with a velvet cloth. Under cross-polarized illumination, a planar arrangement of birefringent cholesteric bands was observed in the collagen films with concentration of 10 mg mL<sup>-1</sup> (Fig. 1B). In contrast, Fig. 1C shows the absence of such optical features for 10 mg mL<sup>-1</sup> collagen solution spaced between a cover slip and a microscope slide with 150 μm spacers in between under cross-polarized light. The complete extinction of light in this image indicates the random orientation of fibrils in the absence of shear force, thus highlighting the important role of shear force in the formation of aligned cholesteric bands. Fig. 1D depicts the trajectory of fibrillar orientation along the major axis of cholesteric bands.

The degree of alignment of cholesteric bands can be quantified using the order parameter (eqn (1)). As a marker for the alignment strength of the collagen films, we quantify the order parameter (*S*) of the cholesteric bands by evaluating the alignment of individual cholesteric bands. In our experiments, the order parameter for unidirectionally aligned cholesteric bands over an area of 6 cm<sup>2</sup> was determined to be as high as 0.85, suggesting a high degree of alignment.<sup>35,44,45</sup>

$$S = \left\langle \frac{3}{2} \cos^2 \theta - \frac{1}{2} \right\rangle \quad (1)$$

The pitch length, denoting the extent over which a complete rotation of collagen fibrils occurs, was quantified using ImageJ software. Two parallel lines, aligned with the orientation of consecutive dark regions, were delineated, and the perpendicular separation between these two parallel lines was defined as the pitch. The determined pitch value is 11.95 μm, with a standard deviation of 0.556 μm. Fig. S1 and S2 (ESI<sup>†</sup>) display the cholesteric bands in LC collagen films and the quantification of their morphological features.

To further quantify the liquid crystalline nature of the aligned collagen films, observations were conducted using cross-polarized microscopy integrated with a rotating stage. The stage was rotated through small incremental rotations, and the average grayscale intensity of the resulting micrographs

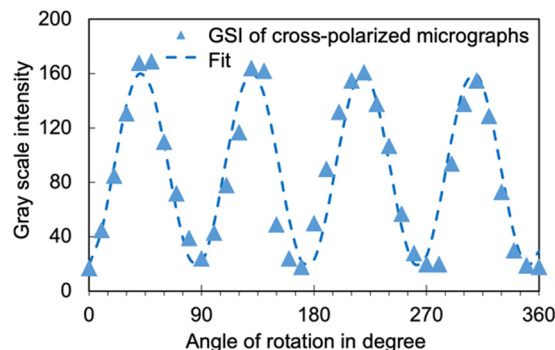


Fig. 2 The average intensity of grayscale value of a sequence of images of LC collagen film under cross-polarized light versus rotation angle (°). The fitted equation is  $A \cos^2(B\theta + C)$ .

was quantified. As shown in Fig. 2, the projection of the overall intensity in the *X-Z* plane is well-described by a  $\cos^2 \theta$  trend (dashed line is the fit of the grayscale intensity versus the rotation angle), indicating the alignment of the collagen stripes along the *x*-axis. This result can alternatively be inferred from the 4-fold radial symmetry plot of the grayscale intensity in Fig. S3 (ESI<sup>†</sup>).

### 2.2. Characterization of the behaviour of HSCs cultured on aligned collagen films

Aligned collagen films were placed in 6-well culture plates and subjected to a culture medium comprised of HSCs and a low concentration of collagen (1 mg mL<sup>-1</sup>). The cells were subsequently incubated at 37 °C for 72 hours. Upon the completion of the growth phase, the morphological properties of the cells were studied. Observations under brightfield microscopy (with an integrated modulation contrast) revealed the directional alignment of HSCs grown on LC collagen films in comparison to the control substrate, as evidenced by Fig. 3A and C. All images of cells in this work use IMC module of the Leica DMIL microscope. IMC (or Hoffman modulation) involves the use of a slit plate to enable oblique illumination and a modulator to enhance contrast, especially for transparent and low-contrast specimens such as cells.<sup>46</sup> Fluorescence imaging further confirmed the directional preference of HSCs when cultured on LC collagen films as opposed to the control sample (shown in Fig. 3B and D).

The order parameter of HSC alignment was determined by using eqn (1), where  $\theta$  represents the angle between the orientation of the long axis of each cell and the average direction of orientation of cholesteric bands. The order parameter was found to be 0.9 (as shown in Fig. 3E).<sup>47</sup> Interestingly, the order parameter of HSCs was slightly elevated in comparison to that of the cholesteric bands themselves—which could be attributed to the tendency of cells to align with their neighbouring counterparts by adhering to the fibronectin network released by the adjacent cells.<sup>48</sup> The order parameter of HSCs cultured on control samples with unaligned collagen was determined to be approximately 0.2. The disparity between the order parameter of cells cultured on control substrate and





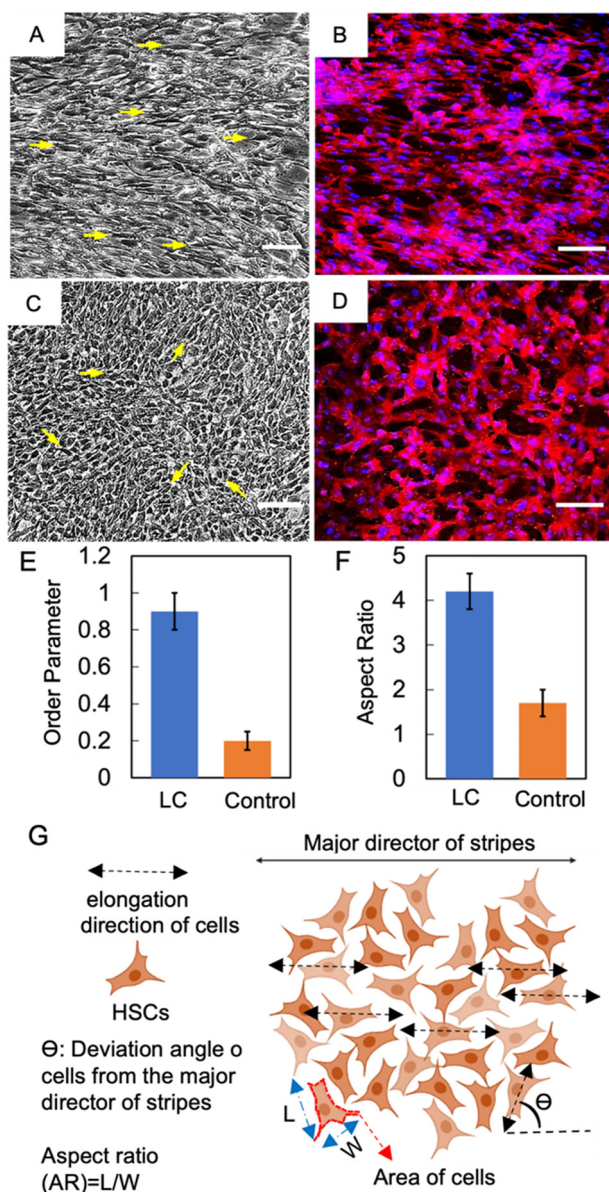


**Fig. 3** Comparison of HSCs behavior on LC and randomly oriented (serving as a control substrate) collagen films (A) and (B) IMC-enhanced brightfield and fluorescent image of HSCs cultured on LC collagen film, respectively. (C) and (D) Bright field and fluorescent image of HSCs, respectively, cultured on the control substrate. Areas marked in blue, and red are the nuclei and actin, which are labeled with Hoechst and Actin Red, respectively. (E) and (F) Comparison of the order parameter, and aspect ratio of HSCs on the LC and control film, respectively. The error bars show the standard deviation of the mean for the average values obtained from the 6 replicates. (G) Illustration of the angle of deviation between the elongation axis of HSCs and the main direction of cholesteric bands. The order parameter and aspect ratio of the cells were calculated by averaging over the entire population in each frame. The scale bars represent 100  $\mu\text{m}$ .

those cultured on aligned collagen film emphasizes the importance of the emergent directional signals to HSCs *via* aligned cholesteric bands to achieve unidirectional orientation of cells.

In addition to the orientation of the HSCs, we quantified the aspect ratio (AR, the ratio of the major axis to the minor axis) of

HSCs-optical micrographs clearly showed the qualitative shape change of the cells grown on aligned collagen when compared to cells grown on control substrates. AR was quantitatively evaluated utilizing the ImageJ software, for a minimum of 100 cells per statistical evaluation (as depicted in Fig. 3F). We find a significant enhancement in the AR of HSCs cultured on LC films, as compared to the control substrates, with the values of 4.2 and 1.7, respectively. While the exact mechanism of the shape change of the cells is beyond the scope of this work, it points to the possibility of sharing of strain between the collagen and cells which has wide scale implications in understanding cellular properties. The sharing of strain is likely brought about by the distortion energy related to the disruption in the orientation of collagen due to the presence of an inclusion, HSCs in this instance. If the strain is coupled to the cellular membrane, the collagen can release some of the strain by stretching the cell membrane.<sup>33</sup> A few other studies have also observed the dependence of AR of HSCs as well as other cell types on the topographic and alignment properties of the substrate.<sup>49–51</sup> Additionally, it has been shown previously that aligned focal adhesion domains are larger and more elongated than non-aligned ones which could in turn manifest in increased aspect ratios of aligned substrates.<sup>52</sup>

### 2.3. Preparation and characterization of large-scale, monodomain 3-D liquid crystalline collagen hydrogels

3-D replication of the native environment is critical to addressing several biological questions as opposed to the simplistic version of using 2-D substrates. Therefore, we subsequently focused on making liquid crystalline collagen hydrogels (LCCHs) by incubating a solution of neutralized concentrated collagen (final concentration of 15  $\text{mg mL}^{-1}$ ), 20% PBS 1 $\times$ , 0.1 wt% glutaraldehyde, and 1  $\mu\text{g mL}^{-1}$  fibronectin on rubbed PI-coated glasses in 6-well plates, while being subjected to a magnetic field with the direction of magnetic field perpendicular to the plane of the glasses (shown in Fig. 4A). The incubation was carried out at 37  $^{\circ}\text{C}$  overnight to promote gelation and crosslinking.

In Fig. 4B, a typical disk-shaped LCCH with a thickness of 5 mm is presented as an example. Fig. 4C presents a cross-polarized optical micrograph of the surface of the LCCH, depicting parallel cholesteric bands with two prominent morphological features, namely tree-like branching and braided structure. The red arrows in Fig. 4C trace the progression of individual cholesteric bands branching into further distinct cholesteric bands and eventually leaving the plane of observation. The extinction of the birefringent cord along the height of the frame results in the braided-like appearance of the cholesteric bands. Fig. 4D illustrates the occurrence of defects with concentrically arranged cholesteric bands on the edge of the hydrogel. These defects arise from the nucleation of disclinations, which is triggered by the curvature-induced stresses present in the hydrogels. The occurrence of these defects can likely be prevented by utilizing larger magnets, wherein the size of the hydrogel is significantly smaller relative to the area of the magnetic field-

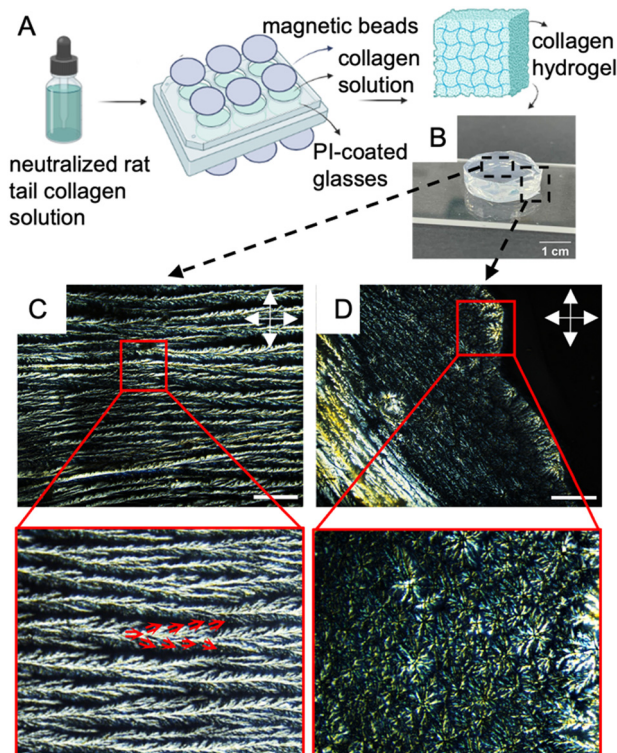


**Fig. 4** Formation and characterization of liquid crystalline collagen hydrogel under applied magnetic field: (A) illustration of a 6-well plate setup in which rubbed polyimide (PI)-coated glasses are placed inside the wells and covered with a neutralized collagen solution ( $10 \text{ mg mL}^{-1}$ ). Subsequently, the setup is subjected to an applied magnetic field and left to crosslink for 2 hours at  $37^\circ\text{C}$ . (B) Visual appearance of the liquid crystalline collagen hydrogel as observed with the unaided eye. (C) and (D) Optical micrographs of the collagen hydrogel, in bulk and edge, respectively, captured using cross-polarized light. Edge-induced disclinations composed of centrally rearranged cholesteric bands is visible in (D). The scale bars represent  $30 \mu\text{m}$ . The double-sided arrows indicate the direction of analyzer and polarizer.

ensuring a homogenous magnetic field distribution throughout the hydrogel.

To quantify the LC order within the hydrogels, we analyze the variations in interference colour as a function of angular orientation. Changes in the interference colour of LCCHs were measured under cross-polarized light as the microscope stage was rotated by  $15^\circ$  increments counter-clockwise (Fig. 5A), with the light intensity and polarizer-analyzer correspondence being fixed. The anisotropy in the optical properties of the hydrogel is depicted in Fig. 5B *via* the  $\cos^2$  fit of gray scale intensity *versus* the rotation angle. To verify the role of magnetic forces in the formation of aligned cholesteric bands in the hydrogels, the same precursor solution of collagen was placed in a 6-well plate containing bare microscope glass, in the absence of a magnetic field, until a gel structure was formed. The complete extinction of light under the cross-polarized optical microscope for this control test (Fig. S4, ESI<sup>†</sup>) demonstrates the isotropic structure of collagen fibrils in the resulted hydrogel.

#### 2.4. Characterization of the behaviour of HSCs cultured in LCCHs

LCCHs were positioned in 6-well culture plates and subjected to a culture medium comprised of HSCs and a low concentration

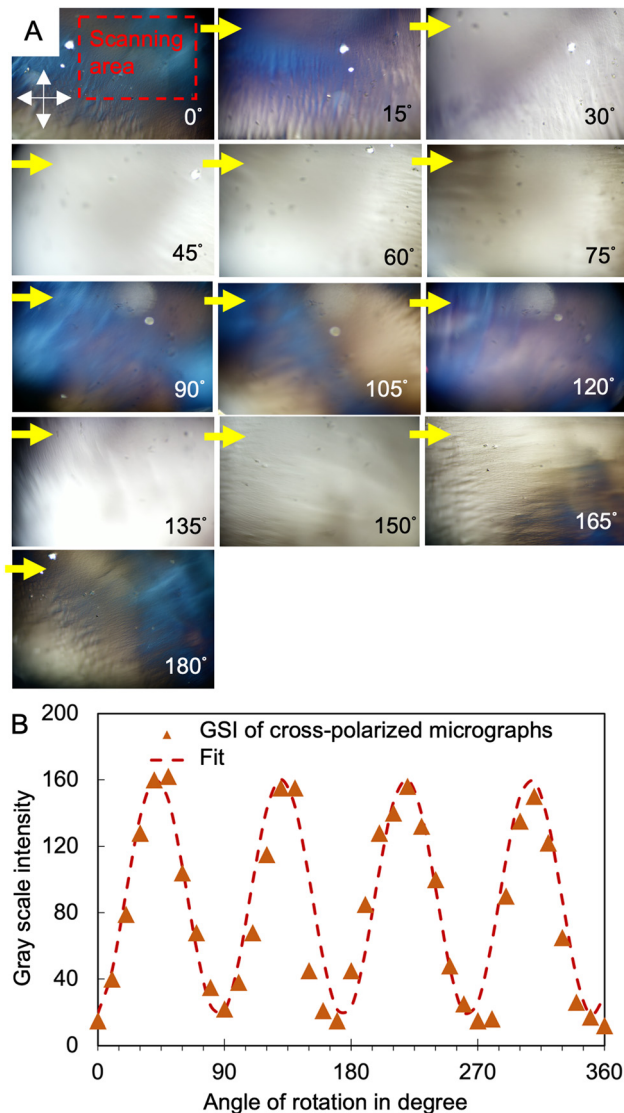


**Fig. 5** (A) Demonstration of range of interference color achieved for collagen hydrogel under cross-polarized light as the microscope platform rotates by  $20^\circ$  progressively in a clockwise manner. Scale bar represents  $100 \mu\text{m}$ . (B) The average intensity of grayscale value of a sequence of images *versus* rotation angle ( $^\circ$ ). The fitted equation is  $A \cos^2(B\theta + C) + D$ .

of collagen ( $1 \text{ mg mL}^{-1}$ ). The cells were subsequently incubated at  $37^\circ\text{C}$  for a period of 72 hours. After the growth phase, the morphological properties of the cells were analysed. Fig. 6A and B are optical micrographs of cells images at a plane about half the thickness of the hydrogel (sliced with a blade). The images were taken after allowing the cells a recovery period as cutting of the hydrogels could result in cell death due to physical trauma. All data in the manuscript is with the hydrogels being incubated for 24 h after slicing, giving the cells time to recover from any mechanical damage caused by the cutting process. These images provide evidence that HSCs grown on LCCHs also exhibited directional alignment when compared to the control substrate. The cells cultured within LCCHs exhibited an order parameter of 0.88, whereas those cultured on the controlled collagen hydrogels displayed a value of 0.1 (Fig. 6C). Fig. 6D





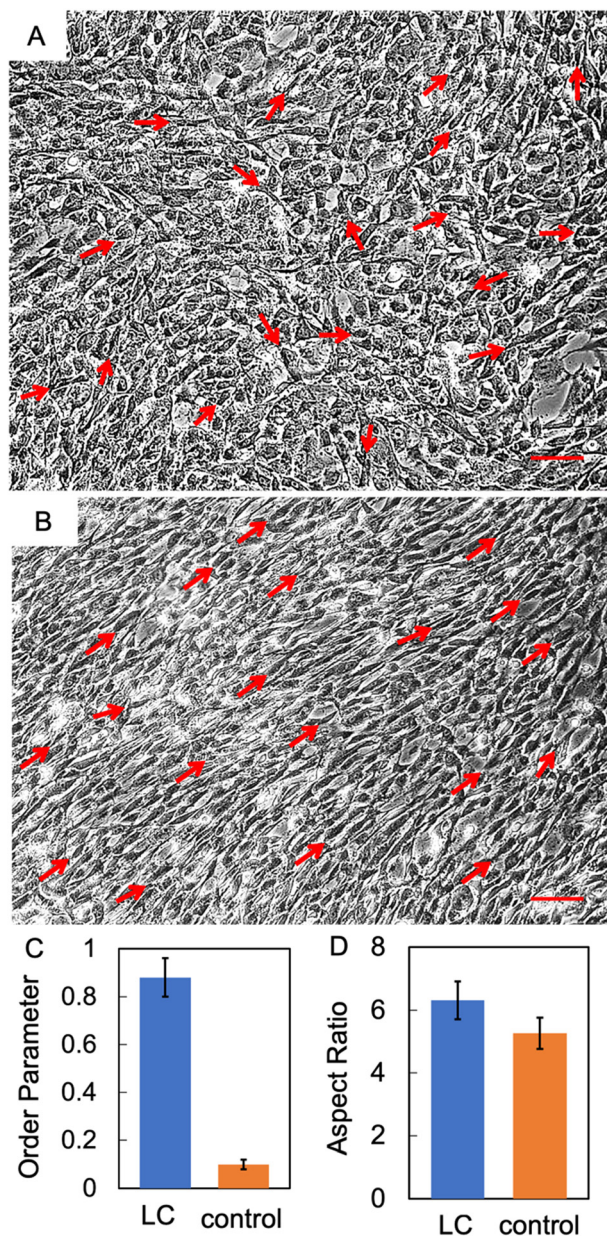


**Fig. 6** IMC-enhanced brightfield images of HSCs cultured on (A) random and (B) LC hydrogel, respectively. Scale bar is 100  $\mu\text{m}$ . (C) and (D) Comparison of the order parameter, and aspect ratio of HSCs on LC and randomly oriented (serving as a control substrate) collagen hydrogels, respectively, cultured on the LC and control collagen hydrogels. The error bars show the standard deviation of the mean for the average values obtained from the 6 replicates.

shows the comparison of the aspect ratio for cells cultured on LCCHs and control hydrogels. The aspect ratio for HSCs on LCCH was measured at 6.31, compared to the control sample with an aspect ratio of 5.26. Notably, we observed that some cells did not exhibit the typical elongated, bipolar spindle-like morphology characteristic of Schwann cells. These variations in shape are highlighted in Fig. S5 (ESI<sup>†</sup>). Specifically, certain cells appeared more circular in shape (as highlighted in red circles in Fig. S5, ESI<sup>†</sup>), which we hypothesize may result from their

protrusion out of the imaging plane, where their orientation perpendicular to the plane gives them a circular appearance in plane of observation. Additionally, we observed some cells displaying ellipsoidal/triangular shapes, which we attribute to cells extending or crawling through the gel at an angle that is neither perpendicular nor parallel to the imaging plane (highlighted in yellow circles in Fig. S5, ESI<sup>†</sup>).

## 2.5. Prediction of order parameter of LCCHs using Monte Carlo-Metropolis algorithm of Ising model

Collagen molecules possess diamagnetic properties which can be used to manipulate the alignment of collagen fibers.<sup>36,53</sup> We model the alignment of the collagen fibers under a magnetic field using the Ising model for ferromagnetic particles as a simplistic model to capture some of the essential features of our observations—namely the ability to align macroscopic domains of collagen at modest magnetic field strengths. The Ising model without a magnetic field was first solved analytically by Lars Onsager in 1944,<sup>54</sup> and it has since been widely used to predict collective behaviour in a variety of fields. In the presence of a magnetic field, the Ising model can be numerically solved using the Metropolis algorithm, which is based on a few assumptions, including the fact that spins can either spin up or down with a tendency to align in the same direction as their neighbouring spins (Fig. S6, ESI<sup>†</sup>).

To measure the distribution of probability for each state, the Boltzmann distribution with the partition function was used (eqn (2) and (3)). Numerically implementing the true-over-sum term at equilibrium in eqn (4) can be challenging. Therefore, we can assume that it is valid for each individual term and enforce this by utilizing eqn (5). To initiate the directional configuration, a random lattice of spins was generated. The system is then subjected to a temperature bath, and the equilibrium state of the orientation distribution of spins is determined numerically (eqn (6)). The energy associated with each state is computed using eqn (7) with a normalization factor  $J$  and summation over multiplication of spin directions for each 4 neighbouring spins. The system undergoes fluctuations governed by the Boltzmann equation until it reaches an equilibrium state.

$$P_{\mu} = \frac{1}{Z} e^{-\beta E_{\mu}} \quad (2)$$

$$Z = \sum_{\mu} e^{-\beta E_{\mu}} \quad (3)$$

$$\sum_{\nu} P_{\mu} P(\mu \rightarrow \nu) = \sum_{\mu} P_{\nu} P(\nu \rightarrow \mu) \quad (4)$$

$$P_{\mu} P(\mu \rightarrow \nu) = P_{\nu} P(\nu \rightarrow \mu) \quad (5)$$

$$\frac{P(\mu \rightarrow \nu)}{P(\nu \rightarrow \mu)} = \frac{P_{\nu}}{P_{\mu}} = e^{-\beta(E_{\nu} - E_{\mu})} \quad (6)$$

$$E_{\mu} = \sum_{\langle i,j \rangle} -J \sigma_i \sigma_j \quad (7)$$

At the equilibrium state, the average spin direction can be determined, which serves as an analogy to the order parameter



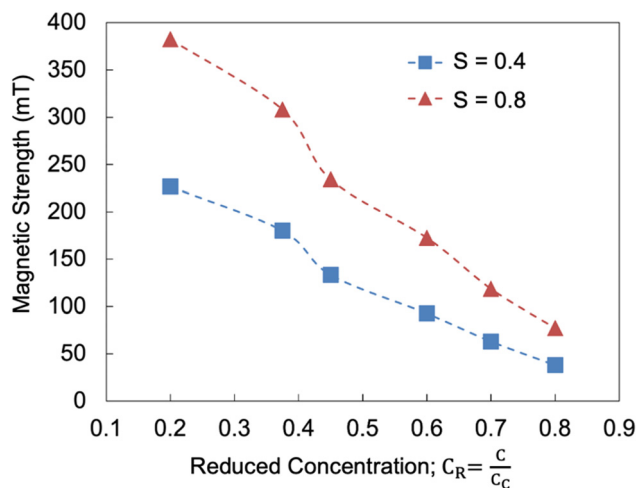


Fig. 7 Simulation-derived plot illustrating the magnetic field strength required for collagen alignment at various concentrations. The order parameter ( $S$ ) is derived from the AASD. The critical concentration for the LC-formation of collagen is  $80 \text{ mg mL}^{-1}$ .

of collagen fibrils. To account for the combined influence of collagen concentration and the strength of the external magnetic field,  $\beta$  in eqn (2) was substituted with a modified parameter (eqn (8)), where  $H_c$  and  $C_c$  represent the critical magnetic field strength and collagen concentration required for the formation of the LC phase.

$$\beta_m = \frac{\beta}{KT} \frac{H}{H_c} \frac{C}{C_c} \quad (8)$$

Fig. 7 depicts the results obtained from computational analysis, showing the magnetic field strength required to align collagen at various concentrations. The plot displays values for two different order parameters, 0.4 and 0.8, derived from the absolute average spin direction (AASD). As the concentration ( $C_R$ ) increases along a constant order parameter (traceable by each curve), the magnetic strength required to align the collagen decreases, indicating enhanced collaborative self-assembly of cholesteric bands at higher concentrations. On the other hand, for a constant  $C_R$ , increasing the magnetic strength raises the order parameter, reflecting a higher degree of alignment.

### 3. Conclusion

Here, we harness the inherent anisotropic viscoelastic properties and diamagnetic susceptibility of collagen to create novel platforms composed of long-range unidirectionally aligned collagen (at concentrations well below the reported critical concentration of collagen to create LC phase). Both, films and hydrogels present with the anisotropy. While the alignment of HSCs along the direction of collagen orientation is intuitively expected, our results also show that, remarkably, the aspect ratio of HSC is a function of the alignment of collagen. IMC enhanced-brightfield and fluorescent microscopy images demonstrate a higher aspect ratio and order parameter in HSCs when cultured on LC platforms as compared to the control

substrates. Our metropolis-based model of alignment of collagen provides guidance on magnetic field strength required to form aligned collagen substrates for a range of concentrations. Future work will explore the 3-D organization of HSCs within the LC-collagen hydrogels. Further, we seek to determine the effects LC orientation of HSC migration as directed migration is a key-step in the deployment of an effective NGC. Long term studies will explore the neuron growth and the formation of the myelin sheet surrounding neurons on the LC substrates.

## 4. Materials and methods

### 4.1. Materials

**4.1.1. Preparation of concentrated collagen solutions.** A stock mixture of collagen type I at a concentration of  $7\text{--}11 \text{ mg mL}^{-1}$  in  $0.02 \text{ N}$  acetic acid was concentrated to prepare solutions with concentrations ranging from  $15$  to  $40 \text{ mg mL}^{-1}$ . The concentration procedure involved dialyzing the stock collagen solution against various concentrations of PEG35k ( $35\text{--}50\%$  w/v) in  $150 \text{ mM}$  acetic acid using  $2 \text{ k MWCO}$  Lyzer cassettes. As the cassette only permitted water to pass through, the ultimate collagen concentration was calculated by deducing the volume of removed water from the initial volume, with the duration of the dialysis serving as the determining factor.

**4.1.2. Preparation of polyamide (PI)-coated substrates.** Microscope slides with a thickness of  $0.5 \text{ mm}$  underwent a thorough cleaning procedure involving sonication in Alconox solution for  $15$  minutes, followed by washing with deionized water and ethanol. Following this, the slides were dried using an air gun and baked at  $150^\circ \text{C}$  for  $1$  hour, after which they were allowed to cool to room temperature. A spin coating technique was then employed, using a  $1:10$  ratio of polyimide (PI) to thinner, with a spin speed of  $1000 \text{ rpm}$  for  $10$  seconds, followed by  $3000 \text{ rpm}$  for  $30$  seconds. The coated slides were subsequently baked at  $250^\circ \text{C}$  for  $2$  hours. The resulting coating thickness was  $\sim 100 \text{ nm}$ .

**4.1.3. Formation of liquid crystalline films.** Collagen fibrils in films were aligned utilizing a shear flow-driven method. The alignment layer comprised of PI was manually rubbed in a unidirectional manner using a velvet cloth, thereby creating parallel guiding grooves. The PI-coated glasses were subsequently washed with isopropyl alcohol and affixed in place using double-sided tape.  $50 \mu\text{L}$  of collagen solution was chosen as the initial volume to cast using a doctor blade to result in films with a thickness of approximately  $150 \mu\text{m}$ —which is the same thickness of the unaligned samples. The shear rate was continually increased until we observed alignment of collagen fibrils. Beyond a shear rate of  $100 \text{ (s}^{-1}\text{)}$ , we did observe an increase in the alignment of the collagen fibrils. The coated substrates were allowed to air dry overnight at room temperature. Birefringence properties of the coatings were measured using an Olympus BX41 optical microscope with cross-polarized light.

**4.1.4. Fabrication of liquid crystalline hydrogels.** The PI-coated substrates were placed in  $6\text{-well}$  glass culture plates. To each well, a solution of neutralized concentrated collagen



(final concentration of  $15 \text{ mg mL}^{-1}$ ), 20% PBS  $1\times$ ,  $0.1 \text{ wt\%}$  glutaraldehyde, and  $1 \mu\text{g mL}^{-1}$  fibronectin was added. Two magnetic beads were placed on the top and bottom of the wells to induce the alignment of collagen fibrils in the direction perpendicular to the magnetic field, thereby promoting a parallel orientation with the grooves. The culture plates were then incubated at  $37^\circ\text{C}$  overnight to facilitate the gelation and crosslinking of the collagen.

**4.1.5. Cell culturing human Schwann cells (HSCs) on collagen substrates.** HSCs from ATCC were cultured in a complete culture medium solution prepared with Dulbecco's modified Eagle's medium from Sigma Aldrich (Cat. #D5648), supplemented with 10% fetal bovine serum from Gibco (Cat. #10-437-028), and 1% penicillin-streptomycin from Sigma-Aldrich (Cat. #P4333), along with sodium bicarbonate and sodium pyruvate. The cells were incubated in a humid incubator at  $37^\circ\text{C}$  with an air atmosphere containing 5%  $\text{CO}_2$  for 72 h. Nearly confluent samples ( $\sim 82\%$ ) were used for analysing the data presented here. Initial cell seeding density was initial cell seeding density of 10 000 cells per  $\text{cm}^2$ . In case of collagen hydrogels, the hydrogels were sliced transversely for imaging, ensuring that the slices were thin enough to allow adequate light transmission while maintaining the structural integrity of the collagen matrix and the embedded cells. The hydrogels were incubated for 24 h after slicing to give the cells sufficient time to recover from any physical damage caused by the cutting. The images were taken after this incubation period.

**4.1.6. Characterization of morphological and orientational properties of cells using ImageJ software.** Characterization of the orientational profiles of the cells cultured on both collagen films and collagen hydrogels (controls and LC substrates) was performed manually using ImageJ. For each frame, a large population of cells (the number varied depending on cell density in each frame) was analyzed. For aspect ratio determination, the following steps were followed. The image was magnified sufficiently to distinguish the cell boundaries at the pixel level. The cell's long axis was determined by drawing a line from one end to the other, and the length was recorded. The width of the cell was measured by drawing a perpendicular line across the short axis, from one edge to the other. The aspect ratio for each cell was calculated as the ratio of the length to the width. These individual aspect ratios were then averaged across the cell population to obtain the aspect ratio for the sample. Regarding the order parameter, the absolute deviation of the long axis of each cell from the nematic director was calculated—first we measure the angles of the cells with respect to an arbitrary line (which is roughly the line they appeared to be aligned) and taking an average of the deviations to find the director. Then, we measure the angles of each cell with respect to the director.

**4.1.7. Instruments.** The morphology of collagen substrates was observed using Olympus BX41 microscope integrated with a rotating stage. Bright field microscopy as well as fluorescent microscopy were used to observe the morphology of HSCs upon culturing. Ossila spin coater was used to apply the polymer solution on the microscope slides. Imaging of cells was performed with a Leica DMIL LED inverted routine fluorescence

microscope which is equipped with an integrated modulation contrast.

## Data availability

Optical and fluorescence microscopy images can be provided upon request to the corresponding author.

## Conflicts of interest

There are no conflicts to declare.

## Acknowledgements

KN acknowledges funding from Arkansas Biosciences. LH acknowledges funding from National Cancer Institute (NCI) Transition Career Development Award (K22-CA237857).

## References

- 1 B. V. Lien, N. J. Brown, S. C. Ransom, B. M. Lechrich, S. Shahrestani, A. R. Tafreshi, R. C. Ransom and R. Sahyouni, Enhancing peripheral nerve regeneration with neurotrophic factors and bioengineered scaffolds: A basic science and clinical perspective, *J. Peripher. Nerv. Syst.*, 2020, 25(4), 320–334.
- 2 R. López-Cebral, J. Silva-Correia, R. Reis, T. Silva and J. Oliveira, Peripheral nerve injury: current challenges, conventional treatment approaches, and new trends in biomaterials-based regenerative strategies, *ACS Biomater. Sci. Eng.*, 2017, 3(12), 3098–3122.
- 3 S. G. Van Neerven, L. Krings, K. Haastert-Talini, M. Vogt, R. H. Tolba, G. Brook, N. Pallua and A. Bozkurt, Human Schwann cells seeded on a novel collagen-based microstructured nerve guide survive, proliferate, and modify neurite outgrowth, *BioMed Res. Int.*, 2014, 2014, DOI: [10.1155/2014/493823](https://doi.org/10.1155/2014/493823).
- 4 H. Takeya, S. Itai, H. Kimura, Y. Kurashina, T. Amemiya, N. Nagoshi, T. Iwamoto, K. Sato, S. Shibata, M. Matsumoto, H. Onoe and M. Nakamura, Schwann cell-encapsulated chitosan-collagen hydrogel nerve conduit promotes peripheral nerve regeneration in rodent sciatic nerve defect models, *Sci. Rep.*, 2023, 13(1), 11932.
- 5 D. Gupta, J. Venugopal, M. P. Prabhakaran, V. G. Dev, S. Low, A. T. Choon and S. Ramakrishna, Aligned and random nanofibrous substrate for the in vitro culture of Schwann cells for neural tissue engineering, *Acta Biomater.*, 2009, 5(7), 2560–2569.
- 6 M.-M. Giraud-Guille, E. Belamie, G. Mosser, C. Helary, F. Gobeaux and S. Vigier, Liquid crystalline properties of type I collagen: Perspectives in tissue morphogenesis, *C. R. Chim.*, 2008, 11(3), 245–252.
- 7 J. E. Kirkwood and G. G. Fuller, Liquid Crystalline Collagen: A Self-Assembled Morphology for the Orientation of Mammalian Cells, *Langmuir*, 2009, 25(5), 3200–3206.





- 8 J. C. Price, P. Roach and A. J. El Haj, Liquid Crystalline Ordered Collagen Substrates for Applications in Tissue Engineering, *ACS Biomater. Sci. Eng.*, 2016, **2**(4), 625–633.
- 9 M.-M. Giraud-Guille, Liquid crystallinity in condensed type I collagen solutions: a clue to the packing of collagen in extracellular matrices, *J. Mol. Biol.*, 1992, **224**(3), 861–873.
- 10 J. E. Kirkwood, *Liquid crystalline collagen: matrices for oriented cell growth*, Stanford University, 2008.
- 11 R. Ayala-Caminero, L. Pinzón-Herrera, C. A. R. Martinez and J. Almodovar, Polymeric scaffolds for three-dimensional culture of nerve cells: a model of peripheral nerve regeneration, *MRS Commun.*, 2017, **7**(3), 391–415.
- 12 E. Torres-Mejía, D. Trümbach, C. Kleeberger, U. Dornseifer, T. Orschmann, T. Bäcker, J. K. Brenke, K. Hadian, W. Wurst and H. López-Schier, Sox2 controls Schwann cell self-organization through fibronectin fibrillogenesis, *Sci. Rep.*, 2020, **10**(1), 1–17.
- 13 Z. Huang, R. Powell, J. B. Phillips and K. Haastert-Talini, Perspective on Schwann cells derived from induced pluripotent stem cells in peripheral nerve tissue engineering, *Cells*, 2020, **9**(11), 2497.
- 14 Q. Tseng, E. Duchemin-Pelletier, A. Deshiere, M. Balland, H. Guillou, O. Filhol and M. Théry, Spatial organization of the extracellular matrix regulates cell–cell junction positioning, *Proc. Natl. Acad. Sci. U. S. A.*, 2012, **109**(5), 1506–1511.
- 15 J.-M. Bourget, M. Guillemette, T. Veres, F. A. Auger and L. Germain, Alignment of cells and extracellular matrix within tissue-engineered substitutes, *Adv. Biomater. Sci. Biomed. Appl.*, 2013, 365–390.
- 16 B. Lanfer, F. P. Seib, U. Freudenberg, D. Stamov, T. Bley, M. Bornhäuser and C. Werner, The growth and differentiation of mesenchymal stem and progenitor cells cultured on aligned collagen matrices, *Biomaterials*, 2009, **30**(30), 5950–5958.
- 17 G. Babakhanova, J. Krieger, B. X. Li, T. Turiv, M. H. Kim and O. D. Lavrentovich, Cell alignment by smectic liquid crystal elastomer coatings with nanogrooves, *J. Biomed. Mater. Res., Part A*, 2020, **108**(5), 1223–1230.
- 18 G. M. Beattie, J. S. Rubin, M. I. Mally, T. Otonkoski and A. Hayek, Regulation of proliferation and differentiation of human fetal pancreatic islet cells by extracellular matrix, hepatocyte growth factor, and cell–cell contact, *Diabetes*, 1996, **45**(9), 1223–1228.
- 19 F. Guilak, D. M. Cohen, B. T. Estes, J. M. Gimple, W. Liedtke and C. S. Chen, Control of stem cell fate by physical interactions with the extracellular matrix, *Cell Stem Cell*, 2009, **5**(1), 17–26.
- 20 D. Jhala, H. Rather, D. Kedaria, J. Shah, S. Singh and R. Vasita, Biomimetic polycaprolactone-chitosan nanofibrous substrate influenced cell cycle and ECM secretion affect cellular uptake of nanoclusters, *Bioact. Mater.*, 2019, **4**, 79–86.
- 21 C. M. Nelson and M. J. Bissell, Of extracellular matrix, scaffolds, and signaling: tissue architecture regulates development, homeostasis, and cancer, *Annu. Rev. Cell Dev. Biol.*, 2006, **22**, 287–309.
- 22 T. Mseka, J. R. Bamburg and L. P. Cramer, ADF/cofilin family proteins control formation of oriented actin-filament bundles in the cell body to trigger fibroblast polarization, *J. Cell Sci.*, 2007, **120**(24), 4332–4344.
- 23 S. A. Lelièvre and M. J. Bissell, Three dimensional cell culture: the importance of microenvironment in regulation of function, *Reviews in Cell Biology and Molecular Medicine*, 2006.
- 24 W. F. Liu and C. S. Chen, Cellular and multicellular form and function, *Adv. Drug Delivery Rev.*, 2007, **59**(13), 1319–1328.
- 25 L. G. Griffith, Emerging design principles in biomaterials and scaffolds for tissue engineering, *Ann. N. Y. Acad. Sci.*, 2002, **961**(1), 83–95.
- 26 F. Rosso, A. Giordano, M. Barbarisi and A. Barbarisi, From cell–ECM interactions to tissue engineering, *J. Cell. Physiol.*, 2004, **199**(2), 174–180.
- 27 R. O. Hynes, The extracellular matrix: not just pretty fibrils, *Science*, 2009, **326**(5957), 1216–1219.
- 28 T. B. Saw, W. Xi, B. Ladoux and C. T. Lim, Biological tissues as active nematic liquid crystals, *Adv. Mater.*, 2018, **30**(47), 1802579.
- 29 D. Gray, Chiral nematic ordering of polysaccharides, *Carbohydr. Polym.*, 1994, **25**(4), 277–284.
- 30 I.-C. Khoo, *Liquid crystals*, John Wiley & Sons, 2007, vol. 64.
- 31 K. Nayani, P. Rai, N. Bao, H. Yu, M. Mavrikakis, R. J. Twieg and N. L. Abbott, Liquid crystals with interfacial ordering that enhances responsiveness to chemical targets, *Adv. Mater.*, 2018, **30**(27), 1706707.
- 32 J. Y. Kim, K. Nayani, H. S. Jeong, H.-J. Jeon, H.-W. Yoo, E. H. Lee, J. O. Park, M. Srinivasarao and H.-T. Jung, Macroscopic alignment of chromonic liquid crystals using patterned substrates, *Phys. Chem. Chem. Phys.*, 2016, **18**(15), 10362–10366.
- 33 K. Nayani, A. A. Evans, S. E. Spagnolie and N. L. Abbott, Dynamic and reversible shape response of red blood cells in synthetic liquid crystals, *Proc. Natl. Acad. Sci. U. S. A.*, 2020, **117**(42), 26083–26090.
- 34 K. Nayani, R. Chang, J. Fu, P. W. Ellis, A. Fernandez-Nieves, J. O. Park and M. Srinivasarao, Spontaneous emergence of chirality in achiral lyotropic chromonic liquid crystals confined to cylinders, *Nat. Commun.*, 2015, **6**(1), 1–7.
- 35 M. Chernousov and D. Carey, Schwann cell extracellular matrix molecules and their receptors, *Histol. Histopathol.*, 2000, **15**(2), 593–601.
- 36 C. Alliraja, J. R. Rao and P. Thanikaivelan, Magnetic collagen fibers stabilized using functional iron oxide nanoparticles in non-aqueous medium, *RSC Adv.*, 2015, **5**(27), 20939–20944.
- 37 S. A. Khadem and A. D. Rey, Theoretical Platform for Liquid-Crystalline Self-Assembly of Collagen-Based Biomaterials, *Front. Phys.*, 2019, **7**, DOI: [10.3389/fphy.2019.00088](https://doi.org/10.3389/fphy.2019.00088).
- 38 P. De Sa Peixoto, A. Deniset-Besseau, M.-C. Schanne-Klein and G. Mosser, Quantitative assessment of collagen I liquid crystal organizations: role of ionic force and acidic solvent, and evidence of new phases, *Soft Matter*, 2011, **7**(23), 11203–11210.



- 39 A. I. Brown, L. Kreplak and A. D. Rutenberg, An equilibrium double-twist model for the radial structure of collagen fibrils, *Soft Matter*, 2014, **10**(42), 8500–8511.
- 40 L. Onsager, The effects of shape on the interaction of colloidal particles, *Ann. N. Y. Acad. Sci.*, 1949, **51**(4), 627–659.
- 41 S. Varghese, S. Narayanankutty, C. Bastiaansen, G. Crawford and D. Broer, Patterned Alignment of Liquid Crystals by (micro)-Rubbing, *Adv. Mater.*, 2004, **16**(18), 1600–1604.
- 42 C. Peng, Y. Guo, T. Turiv, M. Jiang, Q. H. Wei and O. D. Lavrentovich, Patterning of lyotropic chromonic liquid crystals by photoalignment with photonic metamasks, *Adv. Mater.*, 2017, **29**(21), 1606112.
- 43 H. Baza, T. Turiv, B.-X. Li, R. Li, B. M. Yavitt, M. Fukuto and O. D. Lavrentovich, Shear-induced polydomain structures of nematic lyotropic chromonic liquid crystal disodium cromoglycate, *Soft Matter*, 2020, **16**(37), 8565–8576.
- 44 M. A. Chernousov, S. S. Scherer, R. C. Stahl and D. J. Carey, p200, a collagen secreted by Schwann cells, is expressed in developing nerves and in adult nerves following axotomy, *J. Neurosci. Res.*, 1999, **56**(3), 284–294.
- 45 R. Milner, M. Wilby, S. Nishimura, K. Boylen, G. Edwards, J. Fawcett, C. Streuli and R. Pytela, Division of labor of Schwann cell integrins during migration on peripheral nerve extracellular matrix ligands, *Dev. Biol.*, 1997, **185**(2), 215–228.
- 46 R. Hoffman, The modulation contrast microscope: principles and performance, *J. Microsc.*, 1977, **110**(3), 205–222.
- 47 P. Clark, P. Connolly, A. Curtis, J. Dow and C. Wilkinson, Topographical control of cell behaviour: II. Multiple grooved substrata, *Development*, 1990, **108**(4), 635–644.
- 48 Y. Abiko and D. Brunette, Immunohistochemical investigation of tracks left by the migration of fibroblasts on titanium surfaces, *Cells Mater.*, 1993, **3**(2), 4.
- 49 A. S. Crouch, D. Miller, K. J. Luebke and W. Hu, Correlation of anisotropic cell behaviors with topographic aspect ratio, *Biomaterials*, 2009, **30**(8), 1560–1567.
- 50 K. Anselme and M. Bigerelle, Role of materials surface topography on mammalian cell response, *Int. Mater. Rev.*, 2011, **56**(4), 243–266.
- 51 C. Masciullo, R. Dell'Anna, I. Tonazzini, R. Böettger, G. Pepponi and M. Cecchini, Hierarchical thermoplastic rippled nanostructures regulate Schwann cell adhesion, morphology and spatial organization, *Nanoscale*, 2017, **9**(39), 14861–14874.
- 52 A. Ray, O. Lee, Z. Win, R. M. Edwards, P. W. Alford, D.-H. Kim and P. P. Provenzano, Anisotropic forces from spatially constrained focal adhesions mediate contact guidance directed cell migration, *Nat. Commun.*, 2017, **8**(1), 14923.
- 53 M. Ashokkumar, N. T. Narayanan, A. L. M. Reddy, B. K. Gupta, B. Chandrasekaran, S. Talapatra, P. M. Ajayan and P. Thanikaivelan, Transforming collagen wastes into doped nanocarbons for sustainable energy applications, *Green Chem.*, 2012, **14**(6), 1689–1695.
- 54 L. Onsager, Crystal statistics. I. A two-dimensional model with an order-disorder transition, *Phys. Rev.*, 1944, **65**(3–4), 117.

